*Desalination and Water Treatment*
www.deswater.com
doi: 10.1080/19443994.2014.1002432

57 (2016) 4810–4831
March

Taylor & Francis
Taylor & Francis Group

# Simulation and economic evaluation of small-scale SOFC-GT-MED

Mousa Meratizaman[a], Sina Monadizadeh[b], Majid Amidpour[a,*]

[a]*Faculty of Mechanical Engineering, Department of Energy System Engineering, K.N. Toosi University of Technology, No. 15, Pardis St., Molasadra Ave., Vanak Sq., P.O. Box 11365-4435, Tehran, Iran, Tel. +98 912 8701367; email: Meisam_463@yahoo.com (M. Meratizaman), Tel. +98 912 1055614; email: Amidpour@kntu.ac.ir (M. Amidpour)*
[b]*Faculty of industrial Engineering, North Tehran Branch, Islamic Azad University, P.O. Box 19388-13646, Tehran, Iran, Tel. +98 912 3074726; email: Sina.monadizadeh@gmail.com*

Received 24 July 2014; Accepted 21 December 2014

ABSTRACT

Thermal nature of multiple effect distillation (MED) process causes the integration of a desalination unit with a high-temperature power cycle like gas turbine in combination with the solid oxide fuel cell. The improvement in energy efficiency is achieved as a result of this combination. This configuration can be introduced as an effective system for the electrical energy–freshwater production. The electrical efficiency of solid oxide fuel cell-gas turbine (SOFC-GT) is reported about 60%. Small-scale MED unit is presented as a solution for heat recovery in the 300–1,000 kW range of (size of SOFC) SOFC-GT power cycle. The exhausted heat of SOFC-GT power cycle is used in heat recovery steam generator to produce a required motive steam for the desalination unit. Simulation, parametric studies, and economic analysis of proposed system are carried out to investigate the system performance. Economic analyses are applied based on the annualized cost of system method. Results show that the combination of MED with SOFC-GT power cycle makes the system more economic.

*Keywords:* Solid oxide fuel cell/gas turbine power cycle; Multiple effect distillation; Small-scale power–water unit; Annualized cost of system

## 1. Introduction

Water is one of the most abundant resources on the Earth; it also covers three-fourths of the planet's surface. About 97% of the Earth's water is saltwater laid in the oceans and 3% is freshwater in the poles (in form of ice), ground water, lakes, and rivers. Nearly, 70% of this tiny 3% of the world's freshwater is frozen as glaciers, permanent snow covers, ice, and permafrost [1]. Thirty percent of freshwater is underground; most of it is in deep, hard-to-reach aquifers. Lakes and rivers together contain just a little more than 0.25% of all freshwater [2,3].

According to mentioned concerns, the sustainable supply of freshwater is one of the most prominent issues for governments. Table 1 shows the amount of freshwater resources per capita in selected countries. These resources include rivers inside the country and surface freshwater [4,5].

This table depicts that in terms of freshwater resources, Iran is not in a suitable situation to compare with Turkey and US. It is also observed that Saudi Arabia has the least amount of freshwater resources because of being located in the desert climate.

*Corresponding author.

Table 1
Freshwater resources information per capita

| Country | Freshwater resources (billion cubic meter) | Population (million Person) | Resources per capita (thousand cubic meter) |
|---|---|---|---|
| Germany | 106.734156 | 81.726 | 1.306 |
| Brazil | 5,513.616628 | 196.655014 | 28.037 |
| China | 2,840.14669 | 1,344.13 | 2.113 |
| Iran | 131.4211384 | 74.798599 | 1.757 |
| United States | 2,862.28335 | 311.591917 | 9.186 |
| United Kingdom | 146.955786 | 62.641 | 2.346 |
| Turkey | 232.7011234 | 73.639596 | 3.16 |
| Iraq | 37.31293759 | 32.961959 | 1.132 |
| Saudi Arabia | 2.52742869 | 28.082541 | 0.09 |

Iran contains a lot of saltwater resources due to the special geographical situation. The development of desalination methods can be considered as a solution for this problem. The commercial desalination technologies can be divided into two main categories: the thermal distillation such as multi stage flash (MSF) and multiple effect distillation (MED) and the membrane separation such as reverse osmosis (RO) [6].

Thermal nature of MED and MSF process causes the integration of a desalination unit with a high-temperature power cycle like gas turbine in combination with solid oxide fuel cell. The improvement in energy efficiency is attained as a result of this combination. This configuration can be introduced as an effective system for the electrical energy–freshwater production.

As a result of oil and gas companies' concentration in the south of Iran, the distributed power generation (up to megawatt) by gas turbine and gas engine is prevalent in this area. The energy efficiency of these power generation devices is about 35%, so a great amount of exhausted heat is available and can be applied in cogeneration units like thermal desalination. It should be mentioned that the considered area of the country is suffered from the freshwater resource shortage and the presented configuration can be illustrated as a solution for this problem. One of the important issues making the suggested system more feasible is the low energy price and the great freshwater price in this region.

The combination of thermal desalination unit with the high-temperature power generation cycle has been addressed by many researchers during the last years.

Safi and Korchani [7] worked on the cogeneration application of dual purpose power plant (same as gas turbine power cycle) with the low-temperature water desalination unit same as MED and MSF. It is found that the increase of the power plant leads to more important water production quantities. The use of 120 megawatt gas turbine coupled to the MED technology permits to reach attractive costs around 0.5 US$/m$^3$. Cardona and Piacentino [8] studied the optimal design of cogeneration plants for seawater desalination unit. The reject heat from the power cycle can feed an MSF section, while some power feeds the RO section and the MSF auxiliary equipment; the rest is sold to the grid. The proposed model in this study is flexible and suitable for comparative applications in all Mediterranean countries. Junjie et al. [9] worked on the multi-stage flash seawater desalination unit improvement in the cogeneration power plants. The main improvement ideas of MSF are that part of the flash vapor in flash room is extracted into the next stage to heat the flashing brine and part or all of the inlet crude seawater was replaced by the cooling seawater of power unit. The calculation results show that the gain ratio could be increased by 74.1%, the brine concentration in each stage could be reduced by 21.8% on average, and the mean annual capital cost of freshwater production will decrease by 10.7% in comparison with conventional MSF when the extracting quotient of flash vapor increased to its maximum value (0.773). Shakib et al. [10] studied the simulation and optimization of multi-effect desalination coupled to a gas turbine plant with HRSG consideration. Two heuristic algorithms, namely genetic algorithm and particle swarm optimization, are used in optimization process. The first approach is a global optimization problem, which completely optimize the combined system. The second one, as an innovative method, is a local optimization approach, which optimize HRSG and ME-TVC in two separate stages, while the third approach is a multi-objective optimization. Najafi et al. [11] worked on the exergetic, economic, and environmental analyses and multi-objective optimization of an SOFC-gas turbine hybrid cycle coupled with an MSF desalination system. They illustrated that this integrated technology is expected to be promising in the

near future as the capital costs of SOFCs are decreasing and their operational lifetimes are increasing.

Most of the available literature considered the gas turbine power cycle as the cogeneration system in combination with thermal desalination unit. It is illustrated that the integration of large MED-MSF desalination unit with the gas turbine power cycle is economic [10]. As mentioned above, the special economic and geographical conditions of the south of Iran make the distributed power generation feasible more than other parts of the country. The application of small-scale gas turbine power cycle in the range of 1–5 megawatt is very common for power generation in this area. The overall efficiency of this power plant reaches hardly to 30%. So, lots of exhausted heat are available and can be used in the cogeneration application. Combination of solid oxide fuel cell/gas turbine power cycle is introduced as a solution for efficient power production. The exhausted heat from this cycle is applied to MED unit for freshwater production. Technical and economic evaluation of such a system is considered in this article. The innovative parts of this study can be presented as:

(1) Simultaneous evaluations (economic and thermodynamic) of the SOFC-GT-MED are not considered in any publications.
(2) Small-scale integration system is introduced for the specific condition of the country, which is not considered in the available literature.

## 2. System description

Integration of MED unit with SOFC-GT power cycle is considered in this article. Fig. 1 shows the scheme of the proposed system. The main parts of the system are air compressor, fuel compressor, gas expander, air recuperator, fuel recuperator, combustion chamber, SOFC, heat recovery steam generator (HRSG), and MED unit. The compressed inlet air and fuel are preheated in recuperator. After chemical reactions in fuel cell, the exhaust flow is burnt in the combustion chamber. The hot gas flow is used for power production in gas expander and for heat recovery in air and fuel recuperator. Extra heat of hot flow gas is obtained by HRSG to convert the pressurized water into the saturated steam. Finally, the produced steam is applied into MED unit. There is no need for an extra oxygen and fuel in the combustion chamber while the remaining fuel and oxygen from SOFC are utilized in the combustor to increase the temperature before the gas expander.

## 3. System simulation

### 3.1. Simulation of solid oxide fuel cell

The SOFC model that is developed in the present work is formed based on the tubular design. The initial assumptions in simulation are as follows:

(1) Zero-dimensional models are used in the modeling of fuel cell.
(2) Ideal gas assumption is used in the simulation.
(3) Linear approximation is used for the enthalpy and entropy calculation.
(4) Simulation is set in full-load conditions.

In SOFC, the power is generated through electrochemical reactions. Based on the reforming and shifting reactions, the natural gas is converted into a hydrogen-rich synthesis gas inside the fuel cell. Due to the additional cooling need and the higher cost of external reformer [12], the internal reformer is used and the required steam is derived from the anode outlet channel to support the reforming reaction. The chemical reactions in the cells are shown below:

$$CH_4 + H_2O \rightarrow CO + 3H_2 \quad \text{(Reforming)} \tag{1}$$

$$CO + H_2O \rightarrow CO_2 + H_2 \quad \text{(Shifting)} \tag{2}$$

$$H_2 + \frac{1}{2}O_2 \rightarrow H_2O \quad \text{(Electrochemical)} \tag{3}$$

The equilibrium constants of reforming and shifting processes are directly dependent on the temperature and can be determined from the following equation:

$$\log K = AT^4 + BT^3 + CT^2 + DT + E \tag{4}$$

The constant values can be found in the literature [13]. Using the reformer (or stack) temperature, the equilibrium constants can be calculated easily. In this case, the required steam for the steam reforming reaction is derived from the anode outlet stream. Fig. 2 shows the scheme of SOFC inlet and outlet streams.

where (An) stands for anode and (Ca) stands for cathode. As shown in Fig. 2, a part of anode outlet (steam) is used as a return steam to the anode inlet for reforming of the inlet fuel. In this section, the composition of gas in the fuel channel of anode is calculated. Molar flow rate of anode inlet gases is presented as the following equation [12–15]:

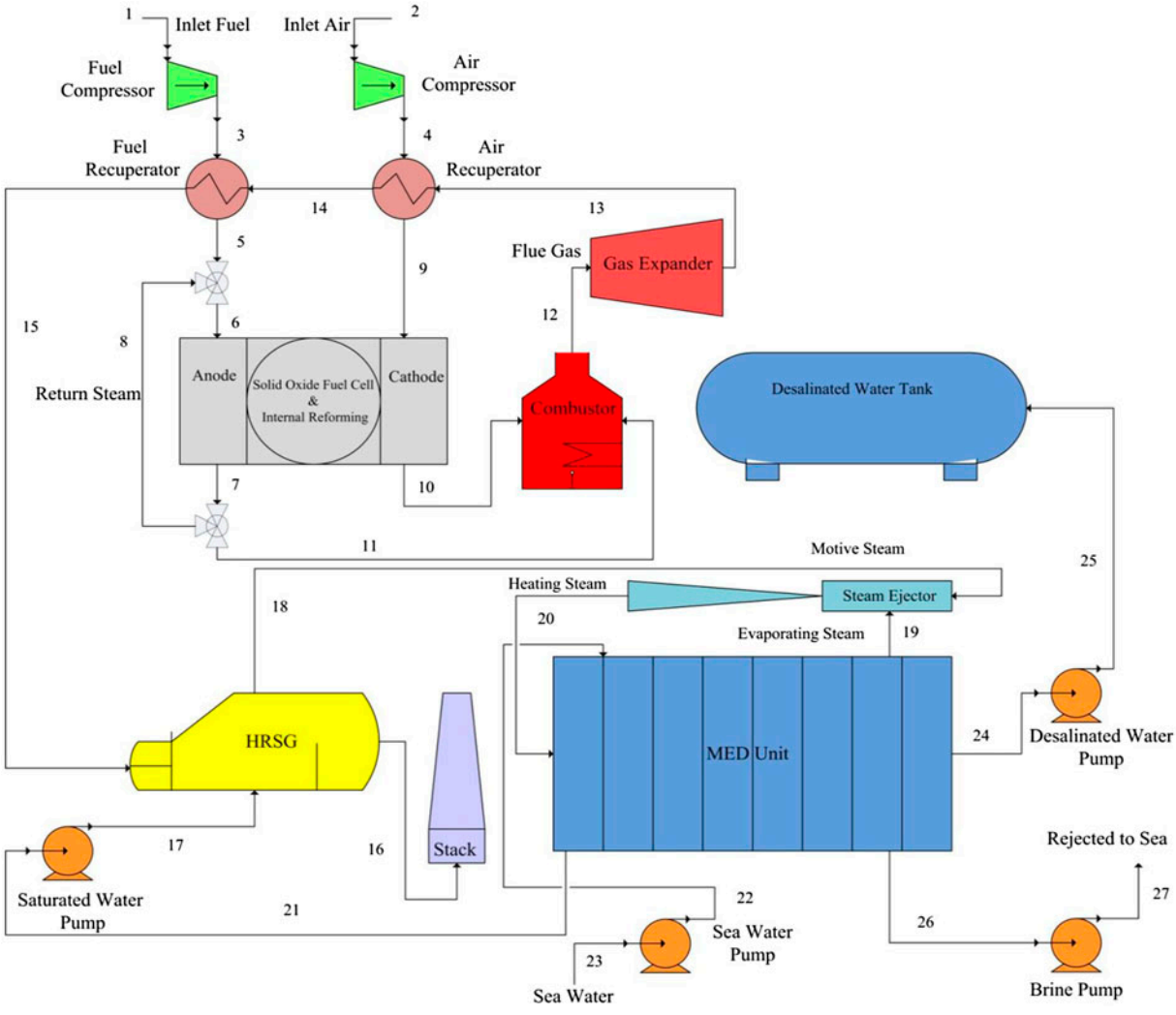


Fig. 1. Scheme of the proposed system.

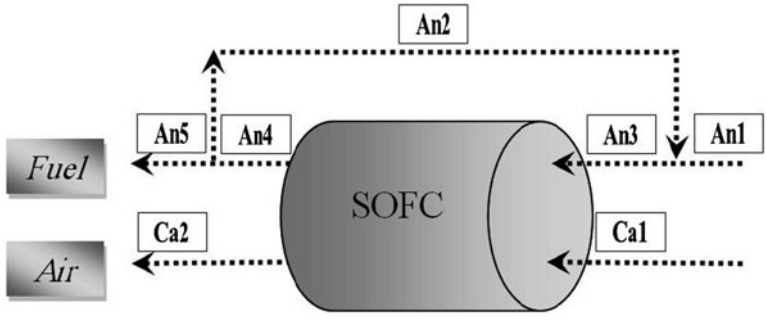


Fig. 2. Solid oxide fuel cell scheme.

$$\dot{n}^{i}_{An1} = X^{i}_{An1} \cdot \frac{\dot{m}_{An1}}{\sum X^{i}_{An1} \cdot M^{i}} \quad (5)$$

After the calculation of return stream from anode, the inlet molar flow rate of fuel channel is computed as follows:

$$\dot{n}^{i}_{An3} = \dot{n}^{i}_{An1} + \dot{n}^{i}_{An2} \quad (6)$$

The outlet molar flow rate of anode (after electrochemical interaction) for every component of gas compound is as below:

$$\dot{n}^{i}_{An4} = \dot{n}^{i}_{An3} + d^{i} \quad (7)$$

In Eq. (7), ($d$) can be calculated as follows:

$$d^{\mathrm{CH_4}} = -x \quad (8\text{-}1)$$

$$d^{\mathrm{H_2O}} = -x - y + z \quad (8\text{-}2)$$

$$d^{\mathrm{CO}} = x - y \quad (8\text{-}3)$$

$$d^{\mathrm{CO_2}} = y \quad (8\text{-}4)$$

$$d^{\mathrm{H_2}} = 3x + y - z \quad (8\text{-}5)$$

$$d^{\mathrm{N_2}} = 0 \quad (8\text{-}6)$$

In above equations, $x$, $y$, and $z$ are the amount of progress (mole/s) in steam reforming, gas shifting, and the electrochemical interaction in solid oxide fuel cell, respectively. The inlet molar flow rate of anode is computed by the integration of Eqs. (7) and (8).

$$\dot{n}_{An3} = \frac{\dot{n}^{i}_{An1} + 2x.(r_e)}{1 - r_e} \quad (9)$$

In Eq. (9), ($r_e$) is the coefficient of return stream from anode. It should be noted that the ratio of every outlet gas from anode in equilibrium condition to the total outlet gases from anode is introduced as below:

$$X^{i}_{\mathrm{eq}} = \frac{\dot{n}^{i}_{An4}}{\dot{n}_{An4}} = \frac{\dot{n}^{i}_{An1} + d^{i}}{\dot{n}_{An1} + 2x} \quad (10)$$

Eq. (10) can be written for every existing gas in outlet gas channel of anode:

$$X^{\mathrm{CH_4}}_{\mathrm{eq}} = \frac{\dot{n}^{\mathrm{CH_4}}_{An1} - x}{\dot{n}_{An1} + 2x} \quad (11\text{-}1)$$

$$X^{\mathrm{CO}}_{\mathrm{eq}} = \frac{\dot{n}_{An1}CO + x - y}{\dot{n}_{An1} + 2x} \quad (11\text{-}2)$$

$$X^{\mathrm{H_2O}}_{\mathrm{eq}} = \frac{\dot{n}^{\mathrm{H_2O}}_{An1} + [-x - y + (\dot{n}^{\mathrm{H_2}}_{An1} + 3x + y) \cdot U_f/(1 - r_e + r_e \cdot U_f)]}{\dot{n}_{An1} + 2x} \quad (11\text{-}3)$$

$$X^{\mathrm{CO_2}}_{\mathrm{eq}} = \frac{\dot{n}^{\mathrm{CO_2}}_{An1} + y}{\dot{n}_{An1} + 2x} \quad (11\text{-}4)$$

$$X^{N_2}_{\mathrm{eq}} = \frac{\dot{n}^{N_2}_{An1}}{\dot{n}_{An1} + 2x} \quad (11\text{-}5)$$

$$X^{\mathrm{H_2}}_{\mathrm{eq}} = \frac{\dot{n}^{\mathrm{H_2}}_{An1} + 3x + y}{\dot{n}_{An1} + 2x} \cdot \left( \frac{(1 - r_e)(1 - U_f)}{1 - r_e + r_e \cdot U_f} \right) \quad (11\text{-}6)$$

In above subequations, $U_f$ is the hydrogen utilization factor that is introduced below:

$$U_f = \frac{\dot{n}_{\mathrm{H_{2,in}}} - \dot{n}_{\mathrm{H_{2,out}}}}{\dot{n}_{\mathrm{H_{2,in}}}} \quad (12)$$

After the definition of oxygen consumption ratio ($U_{\mathrm{ox}}$), the required relations to calculate the inlet and outlet molar flow rate of cathode can be achieved:

$$U_{\mathrm{ox}} = \frac{\dot{n}_{\mathrm{O_{2,in}}} - \dot{n}_{\mathrm{O_{2,out}}}}{\dot{n}_{\mathrm{O_{2,in}}}} \quad (13)$$

According to Eq. (13), the inlet and outlet molar flow rate of cathode are computed as follows:

$$\dot{n}^{O_2}_{\mathrm{Ca1}} = \frac{z}{2 \cdot U_{ox}} \quad (14)$$

$$\dot{n}^{N_2}_{\mathrm{Ca1}} = \frac{z}{2 \cdot U_{\mathrm{ox}}} \cdot \frac{79}{21} \quad (15)$$

$$\dot{n}^{\mathrm{O_2}}_{\mathrm{Ca2}} = \frac{z}{2 \cdot U_{\mathrm{ox}}} - \frac{z}{2} \quad (16)$$

$$\dot{n}^{N_2}_{\mathrm{Ca2}} = \frac{z}{2 \cdot U_{\mathrm{ox}}} \cdot \frac{79}{21} \quad (17)$$

The amount of hydrogen consumption is attained below.

$$z = \frac{i_{\mathrm{cell}} A_{\mathrm{cell}}}{2F} \quad (18)$$

In Eq. (18), $F$, $A$, and $i$ are Faraday coefficient, cell area, and cell current density, respectively. The amount of $x$, $y$, and $\dot{m}_{An1}$ is required to solve above

equations simultaneously and achieve the molar flow rate and the compound percentage of inlet and outlet gases from the anode and cathode.

$$K_r = \exp[-\Delta G_r^0/\mathrm{RT}] = \left[\frac{\left(X_{\mathrm{eq}}^{\mathrm{CO}}\right)\cdot\left(X_{\mathrm{eq}}^{\mathrm{H_2}}\right)^3}{\left(X_{\mathrm{eq}}^{\mathrm{H_2O}}\right)\cdot\left(X_{\mathrm{eq}}^{\mathrm{CH_4}}\right)}\right]\cdot\left(P/P^0\right)^2 \tag{19}$$

$$K_S = \exp[-\Delta G_S^0/\mathrm{RT}] = \left[\frac{\left(X_{\mathrm{eq}}^{\mathrm{H_2}}\right)\cdot\left(X_{\mathrm{eq}}^{\mathrm{CO_2}}\right)}{\left(X_{\mathrm{eq}}^{\mathrm{CO}}\right)\cdot\left(X_{\mathrm{eq}}^{\mathrm{H_2O}}\right)}\right] \tag{20}$$

$$z = \left(\dot{n}_{An3}^{\mathrm{H_2}} + 3x + y\right)\cdot U_f \tag{21}$$

The reversible cell voltage of SOFC is obtained from the Eq. (22).

$$E_{\mathrm{rev}} = E^0 + \Delta E = \frac{-\Delta G^0}{n_e F} + \frac{-\Delta G}{n_e F} = \frac{-\Delta G^0}{2F} + \frac{\mathrm{RT}}{2F}\ln\frac{p_{\mathrm{H_2}}p_{\mathrm{O_2}}^{0.5}}{p_{\mathrm{H_2O}}} \tag{22}$$

In Eq. (22), $E^0$ is the fuel cell open-circuit voltage. In the real fuel cell, the amount of voltage is less than the amount of the reversible voltage. The major reason is the voltage drops that are categorized in three main groups.

(1) The ohmic overpotential.
(2) The activation overpotential.
(3) The concentration overpotential.

According to above terms, the cell voltage of SOFC is calculated as follows:

$$E = E_{\mathrm{rev}} - \left(\eta_{\mathrm{Act}} + \eta_{\mathrm{Ohm}} + \eta_{\mathrm{Conc}}\right) \tag{23}$$

### 3.1.1. Ohmic overpotential

Ohmic losses occur because of the electrical resistance in cathode, anode, electrolyte, and internal layers. These resistances are under the Ohm's law condition and because of series configurations; total resistance is the summation of every resistance in the cell. The SOFC is intensively affected by these losses due to its form and physical shape. The amount of this resistance for SOFC is extremely greater than other kinds of fuel cells. The relations of the Ohmic overpotential are as follows:

$$\eta_{\mathrm{Ohm}} = ir \tag{24}$$

$$r = \delta\rho \tag{25}$$

$$\rho = A\exp\left(\frac{B}{T}\right) \tag{26}$$

The amounts of $A$, $B$, and $d$ of the commercial SOFC (Ni-YSZ), which is considered in this study, are mentioned in Table 2 [16].

### 3.1.2. Activation overpotential

The activation energy and derivative drop, which is known as the activation overpotential, are required to setup the fuel cell and supply the activation energy for all electrochemical interactions and the beginning of current injection from the fuel cell system. The activation overpotential can be obtained from Butler–Volmer equation [16].

$$i = i_0\left\{\exp\left(\beta\frac{n_e F\eta Act}{\mathrm{RT}}\right) - \exp\left(-(1-\beta)\frac{n_e F\eta Act}{\mathrm{RT}}\right)\right\} \tag{27}$$

The calculation of activation overpotential is implicitly possible. $\beta$ is the transfer coefficient which is dependent on the material of the fuel cell and its domain variation is between zero and one. It should be noted that the activation overpotential is computed for the anode and cathode [17].

The amount of $\beta$ is mostly considered 0.5 for the anode and cathode. Using this magnitude, the above formula is simplified as below. Consequently, the equations of activation overpotential for the anode and cathode can be written generally as follows:

$$i = 2i_0\sinh\left(\frac{n_e F\eta Act}{2\mathrm{RT}}\right) \tag{28}$$

$$\eta_{\mathrm{Act,An}} = \frac{2\mathrm{RT}}{n_e F}\sinh^{-1}\left(\frac{i}{2i_{0,\mathrm{An}}}\right) \tag{29}$$

Table 2
The ohmic resistance coefficient for SOFC

| Component | $A$ (W cm) | $B$ (K) | $d$ (cm) |
|---|---|---|---|
| Anode | 0.00298 | 1,392 | 0.01 |
| Cathode | 0.00814 | −600 | 0.19 |
| Electrolyte | 0.00294 | −10,350 | 0.004 |
| Interconnector | 0.1256 | −4,690 | 0.0085 |

$$\eta_{\mathrm{Act,Ca}} = \frac{2\mathrm{RT}}{n_e F}\sinh^{-1}\left(\frac{i}{2i_{0,\mathrm{Ca}}}\right) \tag{30}$$

It is too complicated to calculate the exchange current density precisely. Two semi-experimental relations are used to compute the exchange current density of SOFC.

$$i_{0,\mathrm{anode}} = \gamma_{\mathrm{anode}}\left(\frac{p_{\mathrm{H_2}}}{p_{\mathrm{ref}}}\right)\left(\frac{p_{\mathrm{H_2O}}}{p_{\mathrm{ref}}}\right)\exp\left(-\frac{E_{\mathrm{act,anode}}}{\mathrm{RT}}\right) \tag{31}$$

$$i_{0,\mathrm{cathode}} = \gamma_{\mathrm{cathode}}\left(\frac{p_{\mathrm{O_2}}}{p_{\mathrm{ref}}}\right)^{0.25}\exp\left(-\frac{E_{\mathrm{act,cathode}}}{\mathrm{RT}}\right) \tag{32}$$

$\gamma$ is dependent on the material of anode and cathode electrode, and ($E$) is the amount of activation energy for interaction in cathode and anode. The required magnitudes to calculate the activation overpotential for the tubular fuel cell are shown in Table 3 [17].

#### 3.1.3. Concentration overpotential

Another voltage loss which is evaluated in SOFC is the concentration overpotential and it is related to the time when the fuel cell produces the high current density. In this condition, the partial pressures of hydrogen and air are declined. In other words, the current production rate is not match with the demand and it causes an intensive loss in the fuel cell voltage. So it is recommended to prevent the fuel cell performance in this state. In SOFCs, according to the consuming fuel and the geometry of fuel cell, the limiting current density is defined that after this limitation, the concentration overpotential is at the high level and the operating condition of fuel cell is not suitable, along with lots of losses. Therefore, the fuel cell should not operate in this current density. In this modeling, the calculation of concentration over potential is conducted based on the constant magnitude for the electrical current and using the Fake law. That way, the concentration overpotential is obtained as follows [7]:

Table 3
The magnitude of ($E$ and $\gamma$) for anode and cathode electrodes

| Parameters | Anode | Cathode |
|---|---|---|
| $\gamma$ (A/m$^2$) | $2.13\times10^8$ | $1.49\times10^{10}$ |
| $E_{\mathrm{act}}$ (kJ/mol) | 160 | 110 |

$$\eta_{\mathrm{Conc}} = \frac{\mathrm{RT}}{n_e F}\left(1-\frac{i}{i_l}\right) \tag{33}$$

Finally, the modeling of the amount of produced electrical power by SOFC is computed as follows:

$$\dot{W}_{FC,dc} = IE = (2Fz)E = (i_{cell}A_{cell})E \tag{34}$$

In above equation, $F$ and $z$ are the Faraday coefficient and the consuming hydrogen in the fuel cell, respectively.

### 3.2. Gas turbine, pump, and heat exchanger

Comprehensive relations that are used in GT, pump, and heat exchanger are shown in Table 4.

### 3.3. Combustor

In the combustor, the oxygen mass flow rate is over than the stoichiometric value, so it is assumed that combustion reactions are completely driven. By writing the energy balance equations for the combustor in a control volume, the combustor outlet temperature can be calculated. In this study, the combustor is also modeled with Aspen Hysys commercial software and the same results are obtained.

### 3.4. Heat recovery steam generator

The HRSG that is applied for producing the required motive steam of MED-TVC includes the economizer and evaporator (see Fig. 3). Because the required motive steam is saturated, the boiler does not need the superheater section [10].

The HRSG design in the actual technology is based on the concepts of pinch point and approach point governing the gas and steam temperature profiles. In this study, both pinch point and approach point are included in the modeling. The following equations define these two parameters [10]:

$$T_{\mathrm{ap}} = T_{\mathrm{sat}} - T_{v2} \tag{35}$$

$$T_{\mathrm{pp}} = T_{g1} - T_{v3} \tag{36}$$

Energy and mass balance equations for the economizer and the evaporator could be written as follows:

Evaporator:

$$m_g C_{p,g}(T_{g1} - T_{g1}) = m_{\mathrm{ms}} C_{p,w}(T_{v4} - T_{v3}) \tag{37}$$

Table 4
Relations that are used in gas turbine, pump, and heat exchanger

| Components | Formulas | Parameters |
|---|---|---|
| Compressor | $T_{s,o} = T_i \times \left(\frac{P_o}{P_i}\right)^{\frac{k-1}{k}}$ | Outlet temperature |
| | $\eta = \frac{h_{s,o}-h_i}{h_o-h_i}$ | Isentropic efficiency |
| | $\dot{W} = \dot{m}(h_o - h_i)$ | Required power |
| Gas turbine | $P_o = P_i \times \left(\frac{T_{s,o}}{T_i}\right)^{\frac{k}{k-1}}$ | Downstream pressure |
| | $\eta = \frac{h_o-h_i}{h_{s,o}-h_i}$ | Isentropic efficiency |
| | $\dot{W} = \dot{m}(h_o - h_i)$ | Produced power |
| Pump | $\dot{W} = \frac{\dot{m}(h_o-h_i)}{\eta}$ | Power consumption |
| Recuperator and heat recovery exchanger | $\varepsilon = \begin{cases} \frac{T_{h,o}-T_{h,i}}{T_{h,i}-T_{c,i}} C_h < C_c \\ \frac{T_{c,o}-T_{c,i}}{T_{h,i}-T_{c,i}} C_c < C_h \end{cases}$ | Effectiveness |
| | $A = \frac{\dot{Q}}{U \times F \times \Delta T_{\text{LMTD}}}$ | Area |

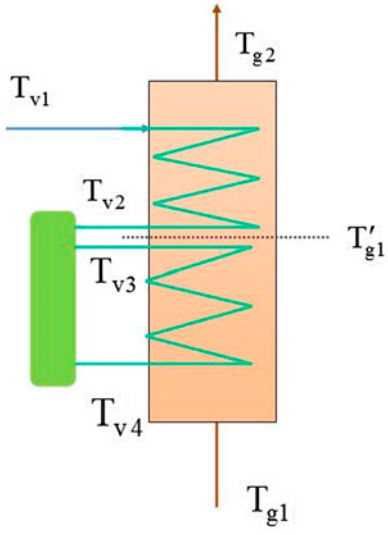


Fig. 3. The scheme of the HRSG.

Economizer:

$$m_g C_{p,g}(T_{g1} - T_{g2}) = m_{\text{ms}} C_{p,w}(T_{v2} - T_{v1}) \quad (38)$$

### 3.5. Multiple effect distillation

Compared with the most widely used MSF desalination, MED thermal vapor compression (MED-TVC) has the advantages of lower corrosion and scaling rates, lower capital cost, longer operation life, and less pumping power consumption [18].

So, thermodynamic simulation of multiple effect distillation with thermo-vapor compressor (MED-TVC) is considered in this section. The plant is parallel/cross-feed and includes evaporators, flashing boxes, steam jet ejector, and finally a condenser. Energy equations are developed and used to examine the performance of the integrated system. Fig. 4 shows the scheme of a six-effect MED-TVC unit.

The following assumptions are considered for the modeling of MED-TVC desalination system:

(1) There is no salt in the produced vapor formed in each effect.
(2) Thermal loss from desalination to the ambient is negligible.
(3) Final reject salinity is assumed less than 72,000 ppm.
(4) Heat transfer area of evaporators 2 to $N$ is the same.
(5) Initially, it was supposed that the temperature difference of all effects is the same that $T_1$ and $T_N$ are the first and the last effect temperature, respectively [19]:

$$\Delta T = \frac{T_1 - T_N}{N-1} \quad (39)$$

$$T_1 = T_s - \Delta T \quad (40)$$

$$T_{i+1} = T_i - \Delta T \quad i = 1, \ldots . N \quad (41)$$

It should be noted that at the end of calculation and solving the energy and mass balance equation, temperature of each effect is computed precisely and it can be different from the first estimation. Fig. 5 shows the inlet and outlet streams of the one effect. Water and salt mass balance for the first effect and the effects 2 to $N$ is as follows [10]:

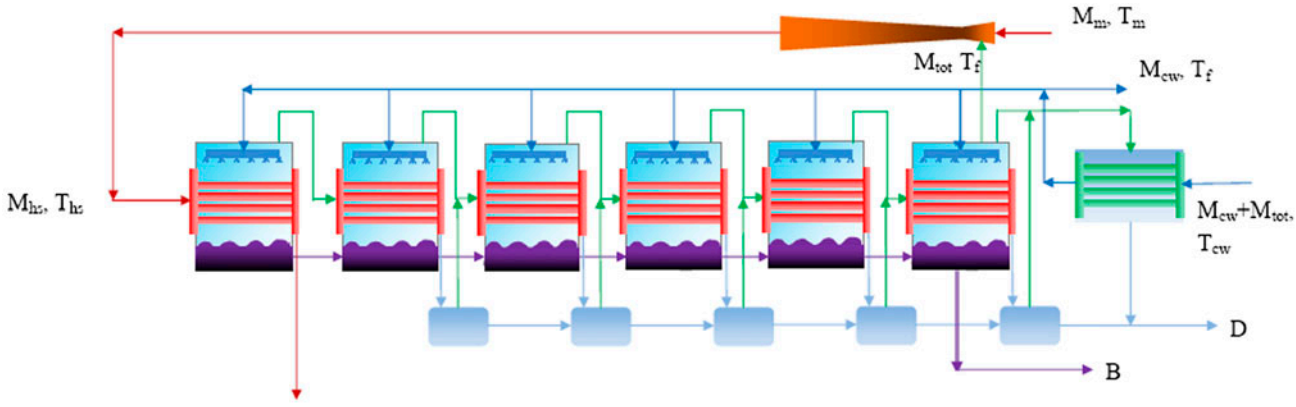


Fig. 4. The scheme of a six-effect MED-TVC unit.

$$B_1 = F - D_1 \tag{42}$$

$$B_i = F + B_{i-1} - D_i \quad i = 2, \ldots, N \tag{43}$$

$$x_1 = \frac{F}{B_1} x_f \tag{44}$$

$$x_i = \frac{F}{B_1} x_f + \frac{B_{i-1}}{B_i} x_{i-1} \quad i = 2, \ldots, N \tag{45}$$

The motive steam of first effect is supplied by the HRSG. So, the energy balance equation of first effect can be written as:

$$D_1 = \frac{1}{L_1}[M_{\mathrm{ms}} L_{\mathrm{ms}} - FC_p(T_1 - T_f)] \tag{46}$$

$$T_f = T_N - \Delta T_{\mathrm{Cond}} \tag{47}$$

It should be mentioned that the vapor is produced by two mechanisms in the effects 2 to $N$:

(1) Boiling.
(2) Flashing.

In these effects, the brine reject of each effect enters to the next effect, and because of decreasing pressure, a small amount of vapor is formed. Another small quantity of vapor is formed in the flash box due to the flashing of distillate condensed in previous effect. The mass flow rate of vapor formed in the flash box is obtained by following equation [20].

$$D'_i = D_{i-1} C_p \frac{T_{v_{i-1}} - T'_i}{L_i} \tag{48}$$

According to the information, the energy balance equation of the effects 2 to $N$ can be written as:

$$D_i = \frac{1}{L_i}\left[(D_{i-1} + D'_{i-1})L_{i-1} - FC_p(T_i - T_f) - B_{i-1}C_p\Delta T\right] \tag{49}$$

The cooling water flow rate is obtained from the following equation:

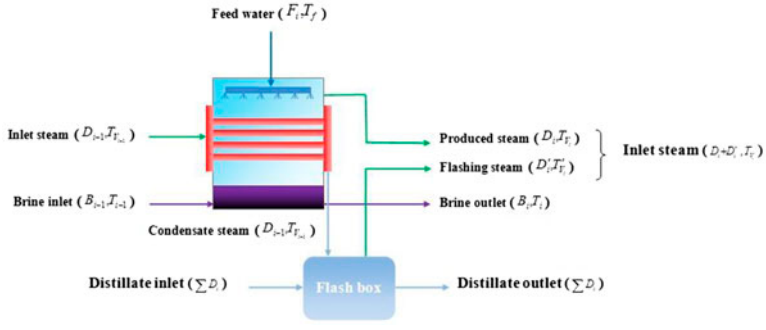


Fig. 5. Inlet and outlet streams of one effect.

$$M_{cw} = \frac{(D_N + D'_N - Mev)Lhs}{C_p(T_f - T_{fcw})} - M_f \quad (50)$$

Heat load of evaporator and condenser can be calculated by equations below:

$$A_1 = \frac{MhsLhs}{U_{e1}(T_{\mathrm{hs}} - T_1)} \quad (51)$$

$$A_i = \frac{(D_{i-1} + D'_{i-1})L_{i-1}}{U_{ei}\Delta T} \quad i = 2, \ldots, N \quad (52)$$

$$A_c = \frac{(D_N + D'_N)L_N}{U_C \mathrm{LMTD}} \quad (53)$$

The specific heat transfer area, the total product, and the brine of ME-TVC are defined as:

$$a = \frac{\sum_{i=1}^{N} A_i + A_c}{D_{tot}} \quad (54)$$

$$M_d = \sum_{i=1}^{N} D_i \quad (55)$$

$$M_b = B(n) \quad (56)$$

Gain output ratio (GOR) is the ratio between the mass of produced freshwater to that of the consumed motive steam:

$$\mathrm{GOR} = \frac{M_d}{M_m} \quad (57)$$

To evaluate the performance of the steam ejector, the entrainment ratio is defined by Shakib et al. [21]:

$$\mathrm{Ra} = \frac{mms}{m_{\mathrm{ev}}} = 0.296 \frac{(Phs)^{1.19}}{(P_{\mathrm{ev}})^{1.04}} \left(\frac{Pms}{P_{\mathrm{ev}}}\right)^{0.015} \left(\frac{\mathrm{PCF}}{\mathrm{TCF}}\right) \quad (58)$$

$$\mathrm{PCF} = 3 \times 10^{-7}(P_{\mathrm{ms}})^2 - 9 \times 10^{-4}(P_{\mathrm{ms}}) + 1.6101 \quad (59)$$

$$\mathrm{TCF} = 2 \times 10^{-8}(T_{\mathrm{ev}})^2 - 6 \times 10^{-4}(T_{\mathrm{ev}}) + 1.0047 \quad (60)$$

So, the heating steam mass flow rate could be calculated by:

$$m_{\mathrm{ev}} = m_{\mathrm{hs}} - m_{\mathrm{ms}} \quad (61)$$

### 3.6. Energy efficiency

This efficiency is based on the first law of thermodynamics and can be defined as follows:

$$\eta_{\mathrm{en}} = \frac{W_{\mathrm{net,GT}} + W_{\mathrm{net,SOFC}} - WDesalination}{m^{\circ}_{\mathrm{CH_4}}(\mathrm{LHV})} \quad (62)$$

Low heating value of natural gas is 55,890 kJ/kg. Required electrical energy for MED consists of:

(1) Electrical energy for recycling the saturated water from MED into HRSG.
(2) Electrical energy for increasing the desalinated water pressure to 4 atmosphere.
(3) Electrical energy for increasing the brine water pressure to 2 atmosphere.
(4) Electrical energy for increasing the seawater pressure to 2 atmosphere.

### 3.7. Economic analysis

An economic evaluation of the introduced configuration is considered in this section. According to the concept of annualized cost of system (ACS), the economic approach is developed in this study. ACS is composed of annualized capital cost $C_{\mathrm{acap}}$, annualized replacement cost $C_{\mathrm{arep}}$, annualized maintenance cost $C_{\mathrm{amain}}$, and annualized operating cost $C_{\mathrm{aope}}$. ACS can be expressed for the presented configuration according to Eq. (63).

$$\begin{aligned}\mathrm{ACS} = {} & C_{\mathrm{acap}}(\mathrm{Air\,Compressor} + \mathrm{Fuel\,Compressor} \\ & + \mathrm{Gas\,Expander} + \mathrm{Combustion\,Chamber} \\ & + \mathrm{SOFC} + \mathrm{HRSG} + \mathrm{Air\,Recuperator} \\ & + \mathrm{Fuel\,Recuperator} + \mathrm{Water\,Pump} + \mathrm{Generator} \\ & + \mathrm{MED\,Effects\,and\,Condenser\,and\,Ejector}) \\ & + C_{\mathrm{arep}}(\mathrm{Air\,Compressor} + \mathrm{Fuel\,Compressor} \\ & + \mathrm{Gas\,Expander} + \mathrm{Combustion\,Chamber} \\ & + \mathrm{SOFC} + \mathrm{HRSG} + \mathrm{Air\,Recuperator} \\ & + \mathrm{Fuel\,Recuperator} + \mathrm{Water\,Pump} + \mathrm{Generator} \\ & + \mathrm{MED\,Effects\,and\,Condenser\,and\,Ejector}) \\ & + C_{\mathrm{amain}}(\mathrm{Air\,Compressor} + \mathrm{Fuel\,Compressor} \\ & + \mathrm{Gas\,Expander} + \mathrm{Combustion\,Chamber} \\ & + \mathrm{SOFC} + \mathrm{HRSG} + \mathrm{Air\,Recuperator} \\ & + \mathrm{Fuel\,Recuperator} + \mathrm{Water\,Pump} + \mathrm{Generator} \\ & + \mathrm{MED\,Effects\,and\,Condenser\,and\,Ejector}) \\ & + C_{\mathrm{ope}}(\mathrm{Labor\,Cost} + \mathrm{Fuel\,Cost} \\ & + \mathrm{Insurance\,Cost})\end{aligned} \quad (63)$$

*3.7.1. Annualized capital cost*

Annualized capital cost of each component (Air Compressor + Fuel Compressor + Gas Expander + Combustion Chamber + SOFC + HRSG + Air Recuperator + Fuel Recuperator + Water Pump+ Generator + MED Effects and Condenser and Ejector) is [22]:

$$C_{\text{acap}} = C_{\text{cap}} \cdot \text{CRF}(i, Y_{\text{proj}}) = C_{\text{cap}} \cdot \frac{i \cdot (1+i)^{Yproj}}{(1+i)^{Yproj} - 1} \tag{64}$$

The capital recovery factor (CRF) is a ratio to calculate the present value of an annuity (series of equal annual cash flows). The annual real interest rate ($i$) is related to the nominal interest rate ($j$) and the annual inflation rate ($f$). Annual interest rate is calculated according to:

$$i = \frac{j - f}{1 + f} \tag{65}$$

In Iran, the nominal interest rate and the annual inflation rate as referred in June 2014 are 20 and 17%, respectively. Therefore, the annual real interest rate of 2.56% is used in this simulation [23].

To calculate the purchase price of equipment, the relations existing in the literature are used. These relations are shown in Table 5.

*3.7.2. Annualized replacement cost*

Annualized replacement cost is the annualized value of all the replacement costs occurring throughout the lifetime of the project. To do this first, future cost of each component should be calculated using following equation:

$$C_{\text{rep}} = C_{\text{cap}}(\text{In Base Year}) \cdot (1+i)^{Yrep} \tag{66}$$

Summation of these costs is equal to $C_{\text{rep}}$. Then, using the following equation, $C_{\text{arep}}$ is calculated.

$$C_{\text{arep}} = C_{\text{rep}} \cdot \text{SFF}(i, Y_{\text{rep}}) = C_{\text{rep}} \cdot \frac{j}{(1+i)^{Yrep} - 1} \tag{67}$$

SFF is the sinking fund factor, which is a ratio to calculate the future value of series of equal annual cash flows. In this article, the amount of replacement cost is assumed to be zero. It means that different components lifetime is equal to the project lifetime.

*3.7.3. Annualized maintenance cost*

System maintenance cost is deemed to be constant every year, and it is related to the lifetime of components. In this study, it is assumed to be 5% of the capital cost of each component.

Table 5
Purchase cost of instrument

| Instrument | Capital cost of instrument | Refs. |
|---|---|---|
| Gas expander | $Z_{\text{Turb}} = W^{\circ}_{\text{Turb}}(1{,}318.5 - 98.328\ln(W^{\circ}_{\text{Turb}}))$ | [24] |
| General heat exchanger (recuperator and HRSG) | $Z_{\text{HRSG}} = 8{,}500 + 409\,(A_{\text{HRSG}})^{0.85}$ | [25] |
| MED effects | $Z_{\text{Eff}} = 201.67 \times Q \times \Delta T_{lm}^{-1} \times dp_t^{0.15} \times dp_s^{-0.15}$ | [26] |
| MED condenser | $Z_{\text{Cond}} = 430 \times 0.582 \times Q \times \Delta T_{lm}^{-1} \times dp_t^{-0.01} \times dp_s^{-0.1}$ | [26] |
| Steam ejector | $Z_{\text{Ejec}} = 16.14 \times 989 \times \dot{m}_{\text{vapor}} \times (\frac{T_i}{P_i})^{0.05} \times P_e^{-0.75}$ | [26] |
| SOFC and other facilities | $Z_{\text{SOFC}} = 1.1(A_{\text{SOFC}})(2.96\,T_{\text{SOFC}} - 1907)$ | [24] |
| Water pump | $Z_{\text{pump}} = 940 \times W^{0.71}_{\text{pump}}(1 + \frac{0.2}{1-\varepsilon_{\text{pump}}})$ | [27] |
| Combustion chamber | $Z_C = \left(\frac{46.08 m^{\circ}_{ca}}{0.995 - \frac{pGT}{pca}}\right)(1 + \exp(0.018 T_{\text{GT}} - 26.4)$ | [28] |
| Generator | $Z_{\text{Gen}} = 60(W^{\circ}_{\text{Turb}} - W^{\circ}_{\text{GC}})^{0.95}$ | [29] |
| Gas compressor | $Z_C = \frac{39.5 \times m^{\circ}}{0.9 - \varepsilon_C}\left(\frac{pdc}{p_{\text{suc}}}\right)\text{In}(\frac{pdc}{p_{\text{suc}}})$ | [28] |

*3.7.4. Annualized operating cost*

Yearly labor cost, fuel cost, and insurance cost of the considered power production system are computed as an annualized operating cost ($C_{ope}$). Table 6 shows the required parameters for the economic evaluation.

*3.7.5. Net present value*

Net present value is the present value of installing and operating the system over its lifetime in the project; it is referred to the lifecycle cost. NPV is calculated according to [30]:

$$\mathrm{NPV} = \frac{\mathrm{ACS}}{\mathrm{CRF}(i, Y_{\mathrm{proj}})} = \mathrm{ACS} \cdot \frac{(1+i)^{Yproj} - 1}{i \cdot (1+i)^{Yproj}} \tag{68}$$

*3.7.6. Levelized cost of product*

Levelized cost of product (LCOP) is the average cost per unit (US$ per Unit of product) of useful total product of the system. It is calculated as follows:

$$\mathrm{LCOP} = \frac{\mathrm{ACS}}{\text{Annual output product of the system}} \tag{69}$$

In this equation, ACS is annualized cost of system (US $/year) and the denominator is the total annual product of the system (unit of product per year). Two main products are produced in this configuration, the electrical energy (kWh) and freshwater (cubic meter). So, for each product, the LCOP can be introduced as follows:

$$\mathrm{LCOP}_{\mathrm{Electrical}} = \frac{\text{ACS of system} - \text{Cost of produced water in the market}}{\text{Annual Electrical Energy production}} \tag{70}$$

$$\mathrm{LCOP}_{\mathrm{Water}} = \frac{\text{ACS of system} - \text{Cost of produced Electrical Energy in the market}}{\text{Annual Freshwater production}} \tag{71}$$

where ACS is the annualized cost of system (US $/year), which includes capital, replacement, annual operating, and maintenance. CRF is capital recovery factor, which is a ratio to calculate the present value of series of equal annual cash flows.

NPV can be calculated separately for capital, replacement, and operating and maintenance cost.

Table 6
The required parameters for the economic evaluation

| Parameters | Magnitude |
|---|---|
| Fuel cost | 0.03 US$ per nominal cubic meter of natural gas |
| Project lifetime | 20 years |
| System availability | 85% |
| Insurance cost | 2% of capital cost |
| Number of labor | 2 |
| Cost of labor | 400 US$ per month |
| Installation cost | 10% of capital cost |
| Cost of product (electrical energy) | 0.03 US$/kWh |
| Cost of product (freshwater) | 0.04 US$/L |
| Tax | 10% |

It should be noted that the LCOP is not a criterion for comparison with the product cost in market because LCOP is calculated based on all costs in the project life time. So introducing a new economic parameter (prime cost) to compare with the market price is essential. Some other economic parameters are introduced below which are used in computing of prime cost.

(1) Capital costs (CC) that are the initial costs of components and cost of installation.
(2) Operating flow costs (OFC) that include operating and maintenance costs, fuel cost, labor cost, and insurance cost calculated for one year.
(3) Volume of product (VOP) that is volume of product in one year.
(4) Prime cost (PC) and it is equal to division of operating flow costs on volume of product.

$$\mathrm{PC} = \mathrm{OFC}/\mathrm{VOP} \tag{72}$$

(1) Cost of product (COP) and it is equal to value of product in the local market.

(2) Summation of product cost (SOPC) and it is equal to multiplication of volume of product and cost of product.

$$\mathrm{SOPC} = (\mathrm{VOP}) \times (\mathrm{COP}) \tag{73}$$

(1) Annual benefit (AB) and it is equal to subtraction of operation flow costs from summation of product cost. It should be noted that the cost of sold electrical energy (when the main product is freshwater) or freshwater (when the main product is electrical energy) is subtracted from annual benefit.

$$\mathrm{AB} = (\mathrm{SOPC} - \mathrm{OFC}) \tag{74}$$

(1) Net annual benefit (NAB) and it is equal to subtraction of tax cost from annual benefit.

(2) Rate of return (ROR) and it is equal to division of net annual benefit on capital costs.

$$\mathrm{ROR} = \frac{\mathrm{NAB}}{\mathrm{CC}} \tag{75}$$

(1) Period of return (POR) and it is equal to division of capital costs on net annual benefit.

$$\mathrm{POR} = \frac{\mathrm{CC}}{\mathrm{NAB}} \tag{76}$$

(1) Additive value (AV) is equal to subtraction of prime cost from cost of product.

$$\mathrm{AV} = \mathrm{COP} - \mathrm{PC} \tag{77}$$

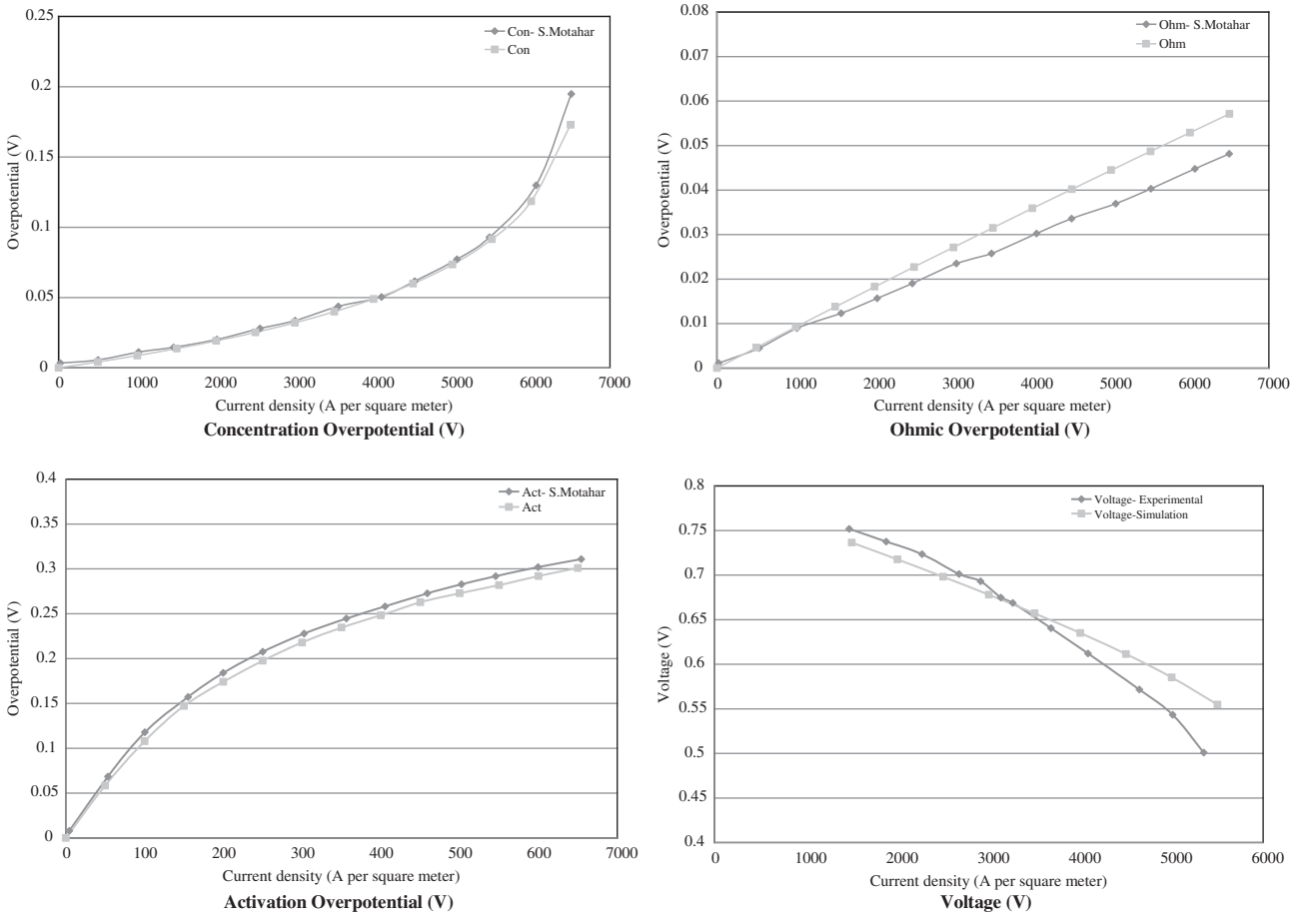


Fig. 6. Different overpotentials and voltage in various current densities.

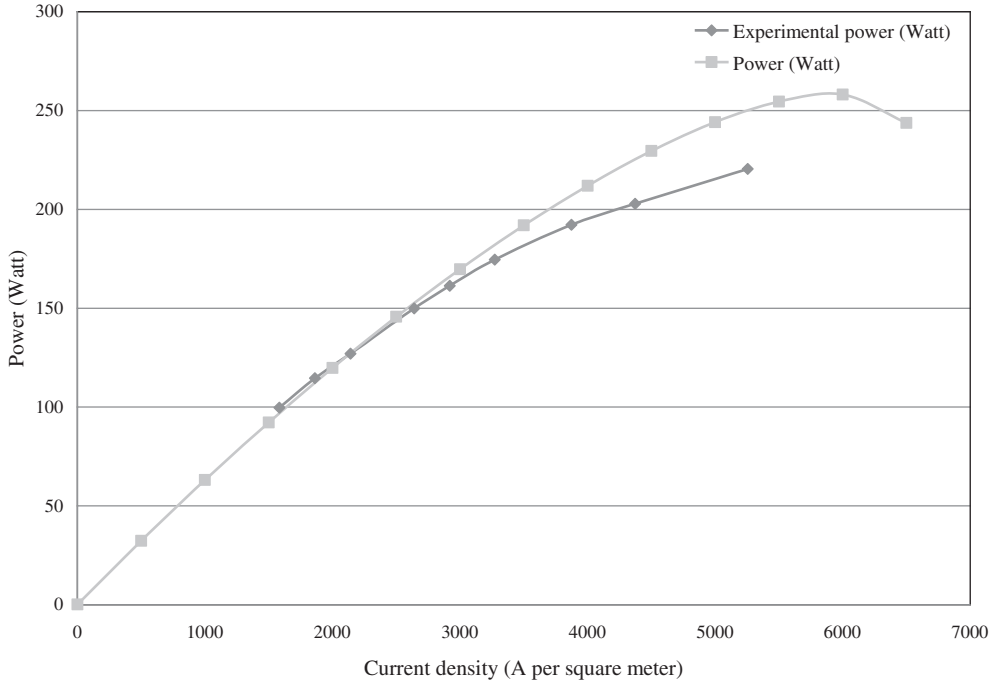


Fig. 7. Power production in various current densities (W).

## 4. Results and discussion

### 4.1. Results of SOFC-GT simulation

Results of SOFC simulation are according to below. The following diagrams (Figs. 6 and 7) show the change of fuel cell voltage and the power production against the change in current density. Table 7 shows the characteristics of simulated fuel cell [15].

Results of simulation are compared with the experimental data and available references [15].

Results of Fig. 6 show that the activation overpotential increases along with current density. The other point that is illustrated in Fig. 6 is the significant increment in concentration overpotential when the SOFC approaches the limiting current density.

In Fig. 7, it is indicated that the output power of SOFC stack rises along with the current density. The maximum stack power output is available in the limiting current density. After this limitation, the output power of SOFC decreases dramatically.

### 4.2. Results of MED system validation

For verification of the MED simulation, a seven-effect MED is considered. Table 8 shows the comparison between the results of this study and the Ref. [31].

Table 7
Characteristics of simulated fuel cell

| Characteristic | Value |
|---|---|
| Limiting current density | 6,000 ($A/m^2$) |
| SOFC net power | 300 (W) |
| Fuel utilization factor | 0.85 |
| Fuel cell temperature | 1,000 (°C) |

### 4.3. Results of SOFC-GT-MED integrated system

To evaluate the performance of triple-integrated system (SOFC-GT-MED) in a kW range, a three-effect MED is chosen and combined with the SOFC-GT power cycle. The size of system is proposed on the basis of SOFC size and in the range of 300–1,000 kW. The specifications of 1 Mw (SOFC-GT-MED) system are shown in Table 9.

Also Table 10 shows the detailed results of system simulation in other capacities of SOFC.

Table 10 illustrates that the desalinated water increases along with the capacity of SOFC. More investigations show that this relation is not totally linear.

It should be noted that the illustrated result in Table 10 is calculated in 8 bars (operating pressure of SOFC-GT). The generated electrical energy and freshwater in different sizes of system and in various

Table 8
Comparison between the presented MED modeling results and available literature

| Calculated effect temperature | | |
|---|---|---|
| Effect number | Present study | Kambiz Ansari et al. |
| 1 | 67.71 | 67.7 |
| 2 | 64.51 | 64.4 |
| 3 | 60.96 | 61.1 |
| 4 | 57.47 | 57.9 |
| 5 | 53.84 | 54.6 |
| 6 | 50.27 | 51.3 |
| 7 | 46.42 | 48 |
| *Total desalinated water* | | |
| Present study | Kambiz Ansari et al. | |
| 24,984 $m^3/d$ | 24,999.12 $m^3/d$ | |
| *GOR* | | |
| Present study | Kambiz Ansari et al. | |
| 8.807 | 8.81 | |
| *Rejected salinity of last effect* | | |
| Present study | Kambiz Ansari et al. | |
| 64,987 | 65,000 | |

operating pressures of SOFC-GT power cycle are shown in Fig. 8.

Results show that the generated power and freshwater in the various operating pressures have the same trend for different sizes of system (SOFC capacity). As a general result, it can be mentioned that the maximum power is achieved in 6 bars operating pressure, while the maximum freshwater is generated in 8 bars. It also shows that the minimum power and freshwater can be obtained at 9 bars and 6 bars, respectively.

### 4.4. Results of economic evaluation

Results of economic evaluation are presented in Table 11. These results are based on the considered assumption in Section (11).

### 4.5. Sensitivity analysis

The sensitivity analysis is conducted in this part to specify the effect of price variations (price of electrical

Table 9
Specifications of 1 MW (SOFC-GT-MED) system

| Air compressor | | Fuel compressor | |
|---|---|---|---|
| Air mass flow (kg/s) | 0.261 | Fuel mass flow (kg/s) | 0.0327 |
| Efficiency | 0.86 | Efficiency | 0.86 |
| Pressure ratio | 8 | Pressure ratio | 8 |
| Inlet pressure (bar) | 1 | Inlet pressure (bar) | 1 |
| Power consumption (kW) | 74.53 | Power consumption (kW) | 15.55 |
| Gas expander | | Combustion chamber | |
| Flue gas mass flow (kg/s) | 0.2937 | Anode outlet mass flow (kg/s) | 0.1447 |
| Inlet temperature (k) | 1,356.15 | Cathode outlet mass flow (kg/s) | 0.149 |
| Outlet temperature (k) | 748.15 | Inlet stream temperature (K) | 1,323.15 |
| Inlet pressure (bar) | 7.8 | Outlet stream temperature (K) | 1,356.15 |
| Efficiency | 0.86 | Inlet pressure (bar) | 7.85 |
| Output power (kW) | 263.2 | Outlet pressure (bar) | 7.8 |
| Solid oxide fuel cell | | | |
| Cell voltage (V) | 0.7802 | Cathode inlet temperature (K) | 713.15 |
| Anode inlet mass flow (kg/s) | 0.068 | Recycle steam mass flow (kg/s) | 0.0353 |
| Cathode inlet mass flow (kg/s) | 0.261 | Stack area ($m^2$) | 657 |
| Inlet pressure (bar) | 7.9 | Number of cell | 7,877 |
| Outlet pressure (bar) | 7.85 | Power density ($W/m^2$) | 1,600 |
| Anode inlet temperature (K) | 883.15 | Utilization factor | 0.86 |
| Multiple effect distillation | | | |
| Number of effects | 3 | Effect one temperature (K) | 341.11 |
| Desalinated water ($m^3/d$) | 11.808 | Effect one pressure (bar) | 0.2593 |
| Inlet seawater salinity (ppm) | 39,000 | Effect two temperature (K) | 337.66 |
| Outlet brine salinity (ppm) | 72,000 | Effect two pressure (bar) | 0.2213 |
| GOR | 5.47 | Effect three temperature (K) | 334.11 |
| Heating steam temperature (K) | 345.15 | Effect three pressure (bar) | 0.1873 |
| Heating steam pressure (bar) | 0.3 | Cooling seawater mass flow (kg/s) | 0.304 |

Note: Table 10 shows the detailed results of system simulation in other capacities of SOFC.

Table 10
The detailed results of system simulation (300–1,000 kW SOFC)

| SOFC power (kW) | 300 | 400 | 500 | 600 | 700 | 800 | 900 | 1,000 |
|---|---|---|---|---|---|---|---|---|
| Net power (SOFC-GT) (kW) | 352.3 | 468.5 | 585.59 | 702.74 | 823.3 | 937.68 | 1,054.12 | 1,171.89 |
| Electrical energy consumption in MED (kWh/d) | 8.994 | 11.778 | 14.724 | 17.652 | 21.144 | 23.652 | 26.508 | 29.52 |
| Generated steam (kg/h) | 27.41 | 35.89 | 44.85 | 53.78 | 64.41 | 72.06 | 80.76 | 89.92 |
| Cell voltage | 0.7802 | 0.7803 | 0.7804 | 0.7804 | 0.7802 | 0.7801 | 0.7805 | 0.7802 |
| Number of cell | 2,362 | 3,153 | 3,945 | 4,736 | 5,515 | 6,292 | 7,110 | 7,877 |
| Desalinated water ($m^3$/d) | 3.5976 | 4.7112 | 5.8896 | 7.0608 | 8.4576 | 9.4608 | 10.6032 | 11.808 |
| Energy efficiency (%) | 65.53 | 64.55 | 64.07 | 63.76 | 65.17 | 64.6 | 64.29 | 64.11 |

power in the market, price of freshwater in the market, and natural gas price) on the period of return and in different sizes of considered system (SOFC capacity and MED number of effect).

*4.5.1. The influence of natural gas price on the period of return*

To investigate the effect of natural gas price on the period of return, a range of [0.03–0.15 US$] is chosen

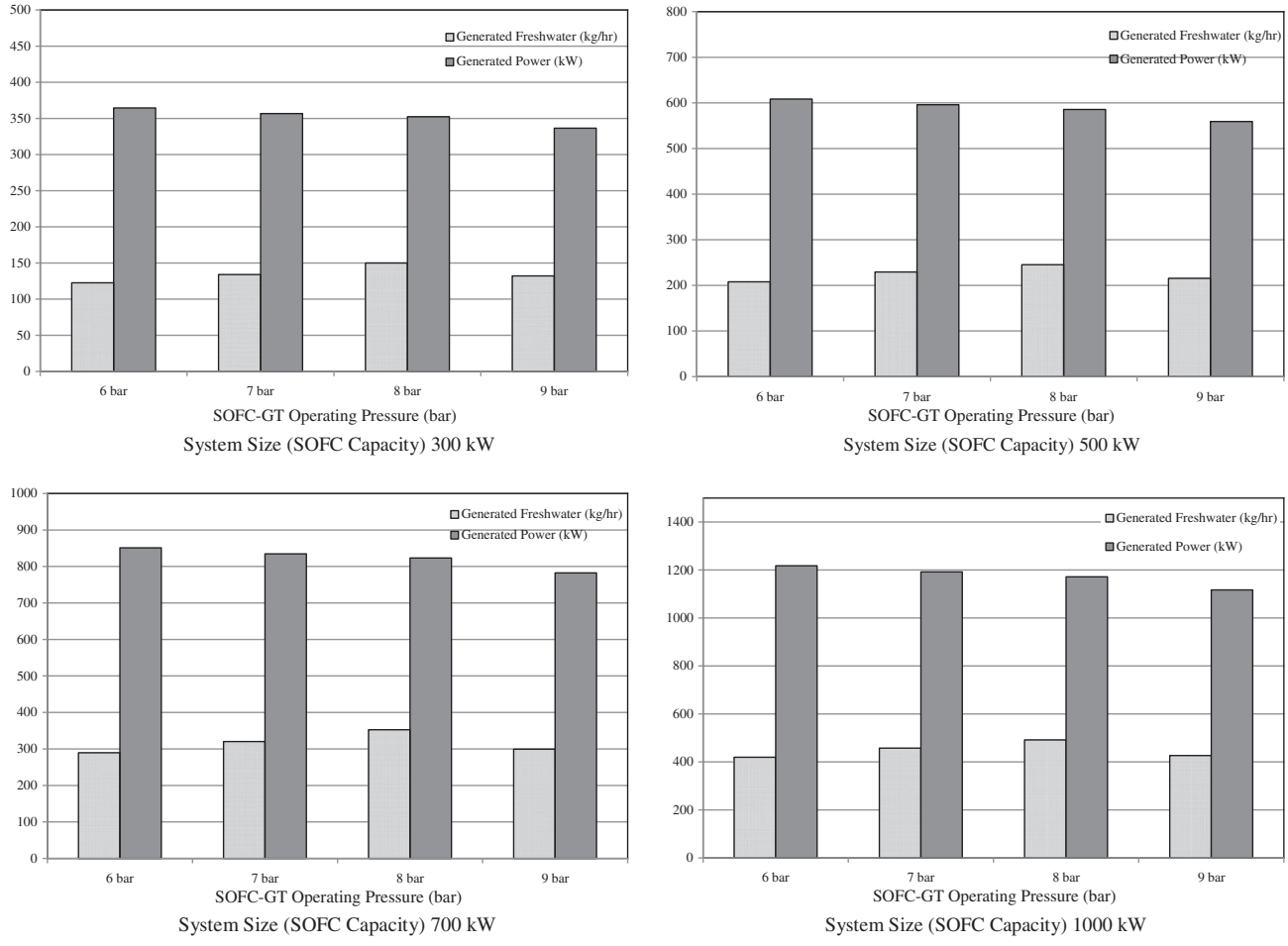


Fig. 8. The generated electrical energy and freshwater in different size of system and in various operating pressure of SOFC-GT power cycle.

Table 11
Results of economic evaluation

| Economic parameter | 300 kW | 400 kW | 500 kW | 600 kW | 700 kW | 800 kW | 900 kW | 1,000 kW |
|---|---|---|---|---|---|---|---|---|
| ACS (US$) | 89,919.18 | 115,290.61 | 140,678.81 | 165,994.47 | 190,785.78 | 215,422.23 | 241,027.78 | 265,726.08 |
| $LCOP_{Water}$ (US$ per liter) | 0.01005 | 0.00727 | 0.0054 | 0.00411 | 0.00262 | 0.00203 | 0.00168 | 0.00107 |
| $LCOP_{Power}$ (US$ per kWh) | 0.0172 | 0.0162 | 0.0155 | 0.0149 | 0.014 | 0.01403 | 0.0139 | 0.0136 |
| PR (US$ per kWh) | 0.02177 | 0.02073 | 0.02008 | 0.01963 | 0.01914 | 0.01893 | 0.01879 | 0.0186 |
| NPV (US$) | 1,393,314.05 | 1,786,448.86 | 2,179,843.68 | 2,572,114.35 | 2,956,260.13 | 3,338,006.37 | 3,734,768.99 | 4,117,473.57 |
| POR (year) | 9.37 | 8.96 | 8.64 | 8.44 | 8.1 | 8.09 | 8.06 | 7.95 |
| Capital cost (US$) | 508,045.34 | 665,497.76 | 823,058.31 | 980,162.62 | 1,137,703.05 | 1,289,609.42 | 1,448,885.11 | 1,601,251.19 |
| Fuel cost (us$ per year) | 11,968.7 | 16,157.07 | 20,347.68 | 24,527.12 | 28,123.54 | 32,323.08 | 36,500.29 | 40,699.83 |
| Tax cost (US$ per year) | 6,621.11 | 9,077.76 | 11,633.72 | 14,186.4 | 17,150.48 | 19,467.17 | 21,953.27 | 24,592.66 |
| Net annual benefit (US$) | 59,590 | 81,699.84 | 104,703.53 | 127,677.67 | 154,354.33 | 175,204.56 | 197,579.5 | 221,333.98 |

and the period of return is computed for 300, 500, and 1,000 kW (size of SOFC). Fig. 9 shows the results of this calculation.

Results show that the period of return increases along with natural gas price. The inclination of these trends rises sharply in the greater natural gas price. The growth of operating flow cost in the constant cost of market (constant revenue) is the main reason for this fact.

*4.5.2. The influence of electrical energy market price on the period of return*

For this purpose, the market cost of electrical energy is changed in the range of [0.03–0.1 US$/kWh] and the period of return is calculated for different sizes of SOFC and in various natural gas prices. Fig. 10 shows the results of this study.

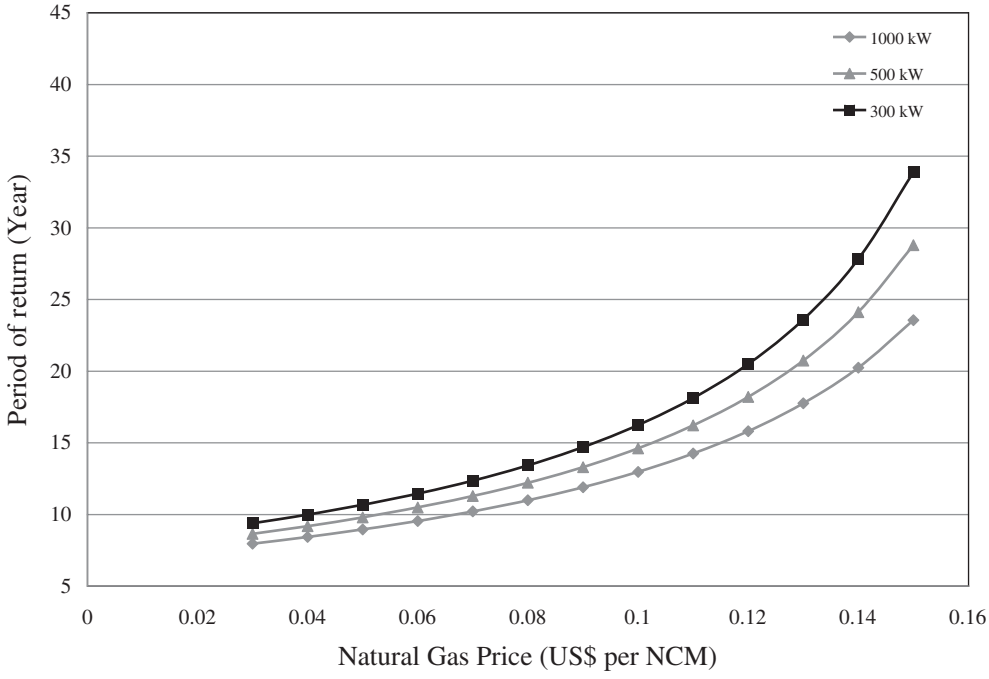


Fig. 9. The influence of natural gas price on the period of return.

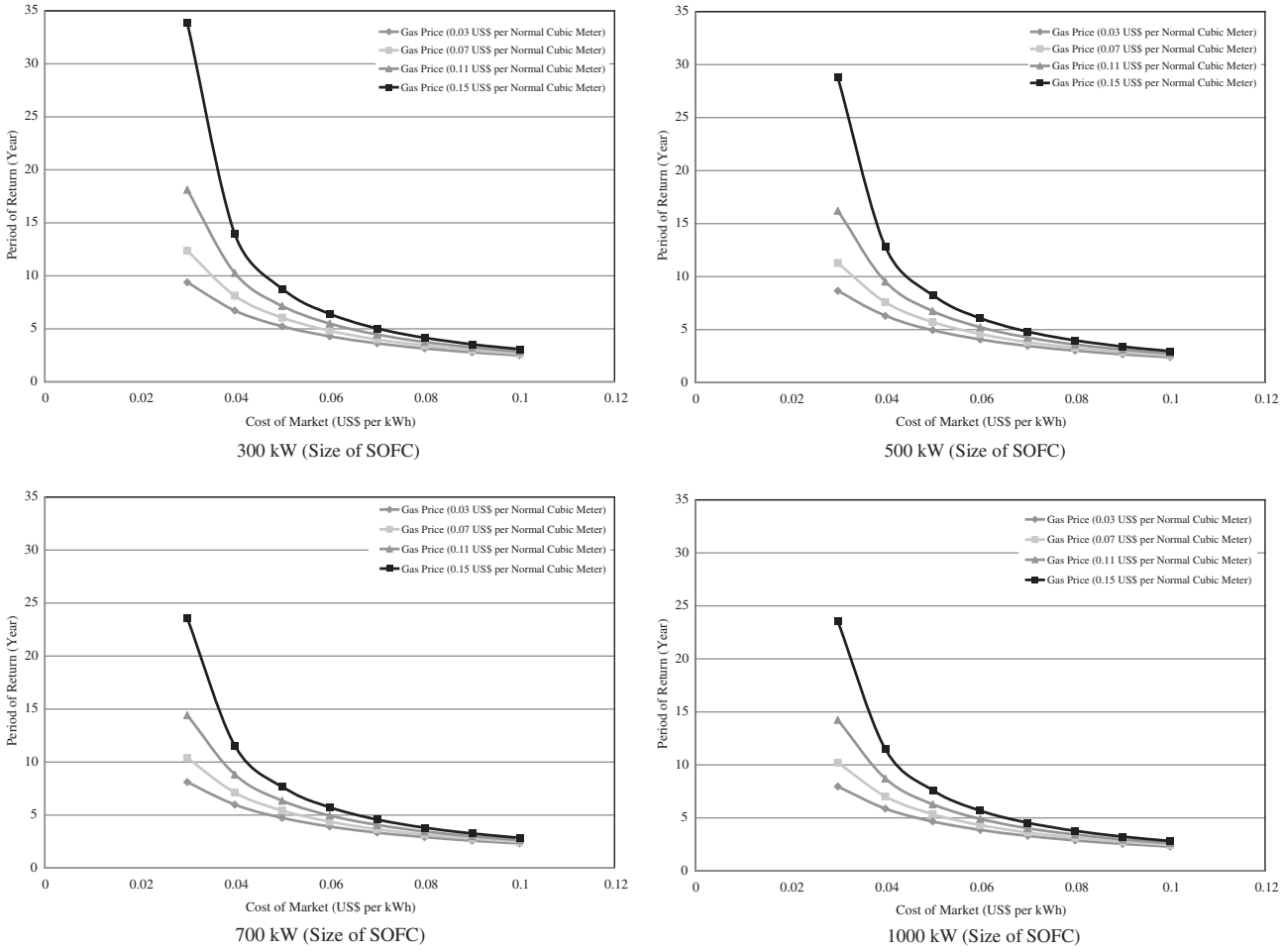


Fig. 10. The influence of electrical energy market price on the period of return.

Results show that the variation in electrical energy market price (especially in the range of 0.03–0.06 US $/kWh) on the period of return is more intensive in the smaller size of system. The main reason of this event is that the growth of electrical energy production is greater than the increase in the system revenue. In contrast, after the electrical energy cost of market (around 0.06 US$/kWh), the rise of system revenue is more than the power production growth. In the current economic condition and prices (0.03 US$/kWh, 0.03 US$ per NCM, and 0.04 US$/L of freshwater), the greater size of system is feasible. It is also indicated that if the market price of electrical energy rises more than 0.06 US$/kWh, the effect of natural gas price and system size can be negligible in system feasibility.

### *4.5.3. The influence of number of MED effect on the period of return*

In this study, 1,000 kW SOFC (size of SOFC-GT) system is considered. The effect number of MED for a constant operating condition of SOFC-GT-MED system is changed from 3 to 7 and the economic condition is investigated. Table 12 shows the amount of desalinated water along with the rise in MED effect number.

Figs. 11 and 12 show the results of period of return calculation along with the change in MED effect number and in various gas prices and market prices of electrical energy. In Fig. 11, the period of return is calculated in different MED effects and along with the variation of natural gas price. For better investigation,

Table 12
The amount of desalinated water along with the rise in MED effect number

| Number of MED effect | Freshwater production (kg/h) |
|---|---|
| 3 | 492 |
| 4 | 600.2 |
| 5 | 691.2 |
| 6 | 771.4 |
| 7 | 846.6 |

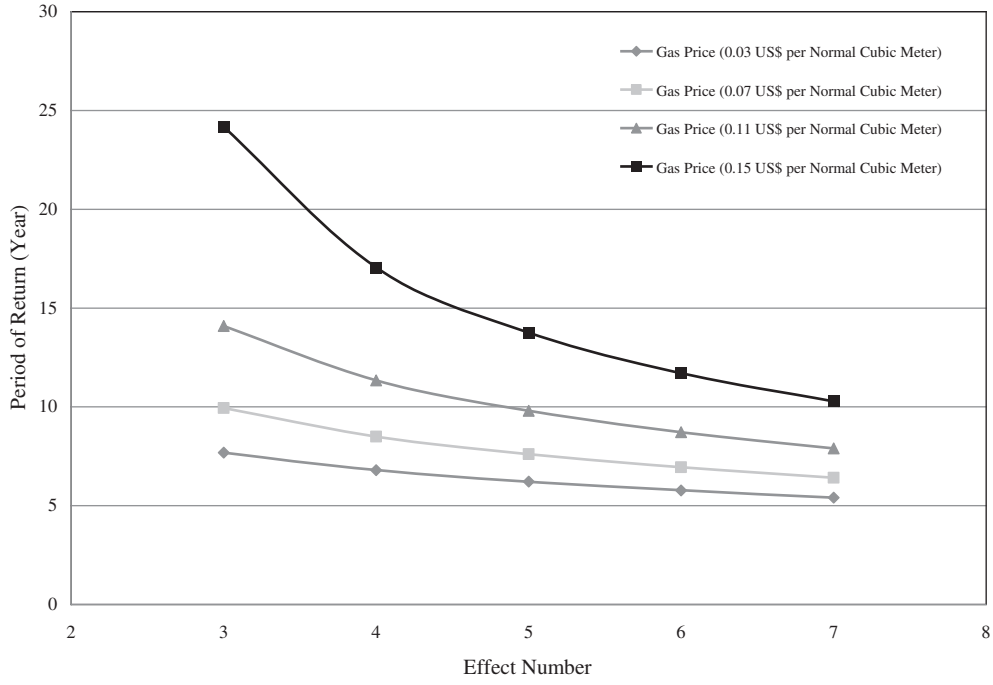


Fig. 11. The results of period of return calculation along with the MED effect changes and in various gas prices.

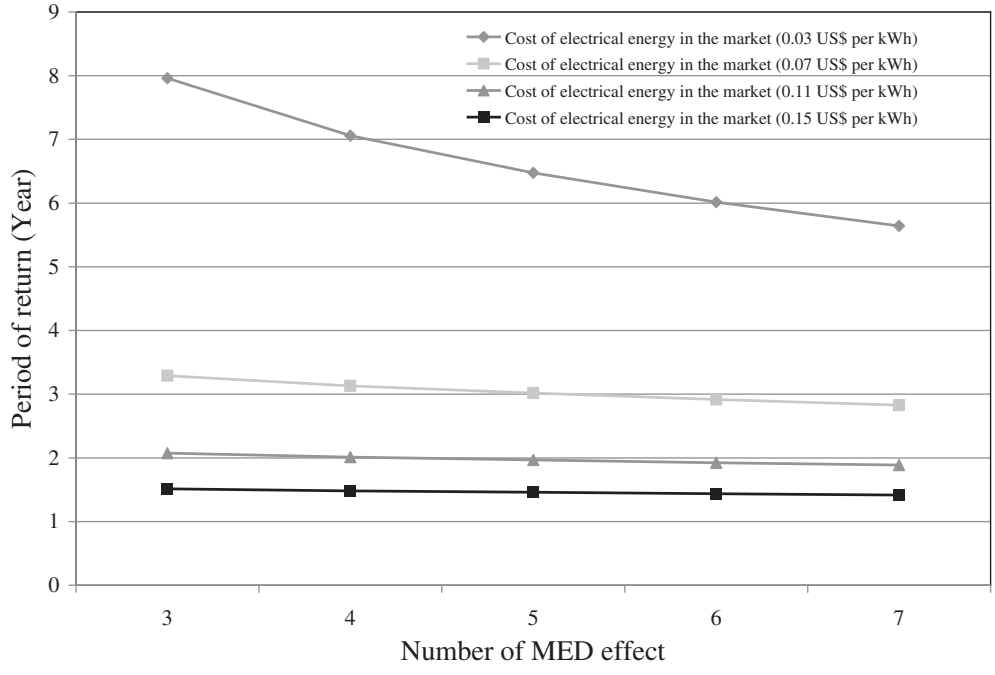


Fig. 12. The results of period of return calculation along with the MED effect changes and in various market prices of electrical energy.

the market price of electrical energy is assumed to be 0.03 US$/kWh. Also in Fig. 12, the period of return is calculated in different MED effects and along with the electrical energy market prices. The natural gas price is assumed to be 0.03 US$ per NCM.

Results of Fig. 11 show that in greater natural gas prices (0.15 US$ per NCM), the variation of number of effect in MED has a tangible influence on the period of return. It also shows that this variation is remarkable in the lower MED effects. The main reason for this event is that the difference between the operating flow cost (fuel price) and the system revenue is negligible in 0.15 US$ per NCM of natural gas price and in three-effect MED. By increasing the number of effect, the amount of revenue of system rises and this leads to an appropriate period of return. The Fig. 12 indicates that the market price of electrical energy has a little influence on the period of return in comparison with the natural gas price effect. This fact is more noticeable in the greater market prices because the difference between the system revenue and the operating flow cost is remarkable enough to conceal the influence of MED effect variation.

## 5. Conclusion

Simulation, parametric studies, and economic analysis of small-scale SOFC-GT-MED unit are carried out to investigate the suggested hybrid system performance in this article. As a result of oil and gas companies concentration in the south of the Iran, the distributed power generation (up to megawatt) by gas turbine and gas engine is prevalent in this area. The energy efficiency of these power generation devices is about 35%, so a great amount of exhausted heat is available and can be applied in cogeneration units like thermal desalination. It should be mentioned that the considered area of the country is suffered from the freshwater resource shortage and the presented configuration can be illustrated as a solution for this problem. One of the important issues making the suggested system more feasible is the low energy price and the great freshwater price in this region. The simulation results show that for a 1,000 kW SOFC-GT system (Size of SOFC), the generated daily freshwater is calculated more than 11 cubic meters. Parametric study shows that the generated power and freshwater in the various operating pressures have the same trend for different sizes of system (SOFC capacity). As a general result, it can be mentioned that the maximum power is achieved in 6 bar operating pressure, while the maximum freshwater is generated in 8 bars. It also shows that the minimum power and freshwater can be obtained at 9 bars and 6 bars, respectively. To investigate the effect of natural gas price on the period of return, a range of [0.03–0.15 US$] is chosen and the period of return is computed for 300, 500, and 1,000 kW (size of SOFC). Results show that the period of return increases along with the natural gas price. The inclination of these trends rises sharply in the greater natural gas price. Finally, the effect number of MED for a constant operating condition of SOFC-GT-MED system is changed from 3 to 7 and the economic condition is investigated. In this condition, the period of return is calculated in the different MED effect numbers and along with natural gas price changes. For better investigation, the market price of electrical energy is assumed to be 0.03 US$/kWh. Results of this study show that in greater natural gas prices (0.15 US$ per NCM), the variation of number of effect in MED has a tangible influence on the period of return. It also shows that this variation is remarkable in the lower MED effects. The main reason for this event is that the difference between the operating flow cost (fuel price) and the system revenue is negligible in 0.15 US$ per NCM of natural gas price and in three-effect MED. By increasing the number of effect, the amount of revenue of system rises and this leads to an appropriate period of return.

## Nomenclature

| | | |
|---|---|---|
| $A$ | — | area, $m^2$ |
| $A$, $B$, $C$, $D$, $E$ | — | coefficient of equilibrium constant |
| $A_i$ | — | heat transfer area of effect $i$, $m^2$ |
| $A_c$ | — | heat transfer area of condenser $i$, $m^2$ |
| $a$ | — | specific heat transfer area, $m^2$ |
| $a$, $b$, $c$ | — | molar flow rate of $CH_4$, CO, and $H_2$ |
| $B$ | — | brine |
| $C_p$ and $C$ | — | specific heat in constant pressure and specific heat, kJ $kg^{-1}$ $K^{-1}$ |
| $C$ | — | cost, US$ |
| $D_i$ and $D'_i$ | — | desalinated water in effect i (boiling and flash), kg $sec^{-1}$ |
| $d$ and $g$ | — | coefficient of resistivity, Ω cm |
| $dp_s$ | — | pressure drop in shell side, Pa |
| $dp_t$ | — | pressure drop in tube side, Pa |
| $E$ | — | cell potential, $V$ |
| $F$ | — | faraday constant |
| $F_t$ | — | correction factor of heat exchanger |
| $F_W$ | — | feed water |
| $f$ | — | annual inflation rate |
| $\Delta G^o$ | — | change in Gibbs free energy at standard $T$, $P$ |
| $h$ | — | enthalpy, kJ $kg^{-1}$ |
| $I$ | — | current, A |
| $i$ | — | current density, A $m^{-2}$, annual real interest rate, and effect number |
| $i_l$ | — | limiting current density, A $m^{-2}$ |
| $i_0$ | — | exchange current density, A $m^{-2}$ |

| | | |
|---|---|---|
| $j$ | — | nominal interest rate |
| $K$, $K_R$, $K_S$ | — | equilibrium constant of reaction, reforming and shifting |
| $k$ | — | heat capacity ratio ($C_p$.$C_v$) |
| $L_i$ | — | latent heat of effect $i$, kJ kg$^{-1}$ |
| $M_i$ | — | molecular weight, kg kmole$^{-1}$ |
| $\dot{m}$ and $M$ | — | mass flow rate, kg s$^{-1}$ |
| $N$ | — | number of effects |
| $N_{\text{cell}}$ | — | SOFC cell number |
| $\dot{n}$ | — | molar flow rate, mole s$^{-1}$ |
| $n_e$ | — | number of electron |
| $P$ and $P^0$ | — | pressure and standard pressure (Pa) |
| $p_i$ | — | partial pressure |
| $\dot{Q}$ | — | transferred heat, kW |
| $Ra$ | — | entrainment ratio |
| $R$ | — | universal gas constant, J mol$^{-1}$ K$^{-1}$ |
| $r$ | — | resistance, Ω |
| $T$ | — | temperature, K |
| $T_{1...N}$ | — | temperature of the effect one to N, K |
| $T'_i$ | — | temperature of flash box in effect $i$, $K$ |
| $U$ | — | overall heat transfer coefficient, kW m$^{-2}$ K$^{-1}$ |
| $U_C$ | — | overall heat transfer coefficient of condenser, kW m$^{-2}$ K$^{-1}$ |
| $U_{ei}$ | — | overall heat transfer coefficient of evaporator i, kW m$^{-2}$ K$^{-1}$ |
| $U_f$ | — | fuel utilization ratio |
| $V$ | — | overpotential, $V$ |
| $\dot{W}$ | — | electrical power, $W$ |
| $x_i$ | — | molar concentration of component $i$ |
| $x$ | — | salinity, ppm |
| $Y_{\text{proj}}$ | — | year of project |
| $Z$ | — | extent of electrochemical reaction, mol s$^{-1}$ and cost, US$ |

Abbreviation

| | | |
|---|---|---|
| AB | — | annual benefit |
| ACS | — | annualized cost of system |
| AV | — | additive value |
| CC | — | capital costs |
| CHP | — | combined heat and power |
| COP | — | cost of product |
| CRF | — | capital recovery factor |
| DC | — | direct current |
| DCHP | — | desalination combined heat and power |
| GA | — | genetic algorithm |
| GOR | — | gain output ratio |
| GT | — | gas turbine |
| HRSG | — | heat recovery steam generator |
| LCOP | — | levelized cost of product |
| LHV | — | low heating value, J mol$^{-1}$ |
| LMTD, lm | — | logarithmic mean temperature difference |
| MED | — | multiple effects distillation |
| MSF | — | multi-stage flash |
| NAB | — | net annual benefit |
| NPV | — | net present value |
| OFC | — | operating flow cost |
| PC | — | prime cost |
| PCF | — | pressure correction factor |
| POR | — | period of return |
| PSO | — | particle swarm optimization |
| ROR | — | rate of return |
| SFF | — | sinking fund factor |
| SOFC | — | solid oxide fuel cell |
| SOPC | — | summation of product cost |
| TCF | — | temperature correction factor |
| TVC | — | thermo-vapor compressor |
| VOP | — | volume of product |

Greek letter

| | | |
|---|---|---|
| $\beta$ | — | transfer coefficient in Butler–Volmer |
| $\varepsilon$ | — | effectiveness |
| $\varepsilon_C$ | — | efficacy of compressor |
| $\delta$ | — | component thickness, $m$ |
| $\rho$ | — | resistivity, Ω cm |
| $\gamma$ | — | pre-exponential coefficient, A/m$^2$ |
| $\eta$ | — | isentropic efficiency |
| $\upsilon$ | — | steam |

Subscript

| | | |
|---|---|---|
| acap and cap | — | annualized capital cost and capital cost |
| act | — | activation |
| amain and main | — | annualized maintenance cost and maintenance cost |
| an, ca | — | anode and cathode |
| aope and ope | — | annualized operating cost and operating cost |
| ap, pp | — | approach point and pinch point |
| arep and rep | — | annualized replacement cost and replacement cost |
| $c$, $h$ | — | cold and hot streams |
| conc | — | concentration |
| cond | — | condenser |
| $c$,$i$ and $c$,$o$ | — | cold stream inlet and outlet |
| $cw$, $d$, $b$ | — | cooling water, desalinated water, and brine |
| $dc$ | — | discharge |
| $en$ | — | energy |
| ev | — | evaporating steam |
| $f$ and $fcw$ | — | feed water and feed cooling water |
| $g$ | — | hot flow gas |
| $h$,$i$ and $h$,$o$ | — | hot stream inlet and outlet |
| hs | — | heating steam |
| $i$ | — | inlet |
| $ms$ | — | motive steam |
| $O$ | — | outlet |
| ohm | — | ohmic |
| $p$,$g$ and $p$,$w$ | — | constant pressure of hot flow gas and water |
| rev | — | reversible |
| sat | — | saturated |
| suc | — | suction |
| $s$,$o$ | — | isentropic outlet |

## References


[1] K. Bourouni, T.B.M. Ben M'Barek, A.A. Al Taee, Design and optimization of desalination reverse osmosis plants driven by renewable energies using genetic algorithms, Renew. Energy 36 (2011) 936–950.

[2] M.A. Eltawil, Z. Zhengming, L. Yuan, A review of renewable energy technologies integrated with desalination systems, Renew. Sust. Energy Rev. 13 (2009) 2245–2262.

[3] S.A. Kalogirou, Seawater desalination using renewable energy sources, Prog. Energy Combust. Sci. 31 (2005) 242–281.

[4] Food and Agriculture Organization, Renewable Internal Freshwater Resources per Capita, 2007–2011. Available from: http://data.worldbank.org/indicator, 19, October 2012.

[5] Pacific Institute, Total Renewable Freshwater Supply by Country. Available from: http://www.worldwater.org/data.html, 19, October 2012.

[6] A.D. Khawaji, I.K. Kutubkhanah, J.M. Wie, Advances in seawater desalination technologies, Desalination 221 (2008) 47–69.

[7] M.J. Safi, A. Korchani, Cogeneration applied to water desalination: Simulation of different technologies, Desalination 125 (1999) 223–229.

[8] E. Cardona, A. Piacentino, Optimal design of cogeneration plants for seawater desalination, Desalination 166 (2004) 411–426.

[9] Y. Junjie, S. Shufeng, W. Jinhua, L. Jiping, Improvement of a multi-stage flash seawater desalination system for cogeneration power plants, Desalination 217 (2007) 191–202.

[10] S.E. Shakib, M. Amidpour, C. Aghanajafi, Simulation and optimization of multi effect desalination coupled to a gas turbine plant with HRSG consideration, Desalination 285 (2012) 366–376.

[11] B. Najafi, A. Shirazi, M. Aminyavari, F. Rinaldi, R.A. Taylor, Exergetic, economic and environmental analyses and multi-objective optimization of an SOFC-gas turbine hybrid cycle coupled with an MSF desalination system, Desalination 334 (2014) 46–59.

[12] S.H. Chan, H.K. Ho, Y. Tian, Modeling of simple hybrid solid oxide fuel cell and gas turbine power plant, J. Power Sources 109 (2002) 111–120.

[13] P. Costamagna, K. Honegger, Modeling of solid oxide heat exchanger integrated stacks and simulation at high fuel utilization, J. Electrochem. Soc. 145 (1998) 3995–4007.

[14] C.O. Colpan, I. Dincer, F. Hamdullahpur, Thermodynamic modeling of direct internal reforming solid oxide fuel cells operating with syngas, Int. J. Hydrogen Energy 32 (2007) 787–795.

[15] S. Motahar, A.A. Alemrajabi, Exergy based performance analysis of a solid oxide fuel cell and steam injected gas turbine hybrid power system, Int. J. Hydrogen Energy 34 (2009) 2396–2407.

[16] S.C. Singhal, K. Kendal, High Temperature Solid Oxide Fuel Cell, Fundamentals, Design and Applications, Elsevier Ltd, Oxford, 2003.

[17] J. Pirkandi, M. Ghassemi, M.H. Hamedi, R. Mohammadi, Electrochemical and thermodynamic modeling of a CHP system using tubular solid oxide fuel cell (SOFC-CHP), J Clean Prod. 29–30 (2012) 151–162.

[18] Y. Wang, N. Lior, Performance analysis of combined humidified gas turbine power generation and multi-effect thermal vapor compression desalination systems Part 1: The desalination unit and its combination with a steam-injected gas turbine power system, Desalination 196 (2006) 84–104.

[19] R.K. Kamali, A. Abbassi, S.A.S. Sadough Vanini, M.S. Saffar Avval, Thermodynamic design and parametric study of MED-TVC, Desalination 222 (2008) 596–604.

[20] H.T. El-Dessouky, H.M. Ettouney, Fundamentals of Salt Water Desalination, Elsevier, Amsterdam, 2002.

[21] S.E. Shakib, M. Amidpour, C. Aghanajafi, Thermodynamic analysis of a combined power and water production system, Proceedings of the ASME 2010 (Turkey), 10th biennial conference on engineering systems design and analysis, vol. 1, pp. 265–273.

[22] Y. Hongxing, Z. Wei, L. Chengzhi, Optimal design and techno-economic analysis of a hybrid solar–wind power generation system, Appl. Energy 86 (2009) 163–169.

[23] Statistics which published by central bank of the Islamic republic of Iran, [June, 2014].

[24] D.F. Cheddie, Thermo-economic optimization of an indirectly coupled solid oxide fuel cell/gas turbine hybrid power plant, Int. J. Hydrogen Energy 36 (2011) 1702–1709.

[25] H. Sayyaadi, R. Mehrabipour, Efficiency enhancement of a gas turbine cycle using an optimized tublar recuperator heat exchanger, Energy 38 (2012) 362–375.

[26] M.H.K. Khoshgoftar Manesh, H. Ghalami, M. Amidpour, M.H. Hamedi, Optimal coupling of site utility steam network with MED-RO desalination through total site analysis and exergoeconomic optimization, Desalination 316 (2013) 42–52.

[27] R. Carapellucci, L. Giordano, A comparison between exergetic and economic criteria for optimizing the heat recovery steam generators of gas-steam power plants, Energy 58 (2013) 458–472.

[28] L. Galanti, A.F. Massardo, Micro gas turbine thermodynamic and economic analysis up to 500 kWe size, Appl. Energy 88 (2011) 4795–4802.

[29] C.A. Gibson, M.A. Meybodi, M. Behnia, Optimization and selection of a steam turbine for a large scale industrial CHP (combined heat and power) system under Australia's carbon price, Energy 61 (2013) 291–307.

[30] M.S. Ngan, C.W. Tan, Assessment of economic viability for PV/wind/diesel hybrid energy system in southern Peninsular Malaysia, Renew. Sust. Energy Rev. 16 (2012) 634–647.

[31] K. Ansari, H. Sayyaadi, M. Amidpour, Thermoeconomic optimization of a hybrid pressurized water reactor (PWR) power plant coupled to a multi effect distillation desalination system with thermo-vapor compressor (MED-TVC), Energy 35 (2010) 1981–1996.